

Ternary Unitary Quantum Lattice Models and Circuits in 2 + 1 Dimensions

Richard M. Milbradt^{1,*}, Lisa Scheller^{1,†}, Christopher Aßmus^{1,‡} and Christian B. Mendl^{1,2,§}

¹Technical University of Munich, School of CIT, Department of Informatics, Boltzmannstraße 3, 85748 Garching, Germany

²Technical University of Munich, Institute for Advanced Study, Lichtenbergstraße 2a, 85748 Garching, Germany

 (Received 1 July 2022; accepted 27 January 2023; published 3 March 2023)

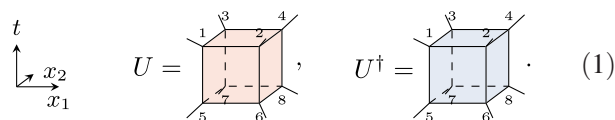
We extend the concept of dual unitary quantum gates introduced in *Phys. Rev. Lett.* **123**, 210601 (2019) to quantum lattice models in 2 + 1 dimensions, by introducing and studying *ternary unitary* four-particle gates, which are unitary in time and both spatial dimensions. When used as building blocks of lattice models with periodic boundary conditions in time and space (corresponding to infinite temperature states), dynamical correlation functions exhibit a light ray structure. We also generalize solvable matrix product states introduced in *Phys. Rev. B* **101**, 094304 (2020) to two spatial dimensions with cylindrical boundary conditions, by showing that the analogous *solvable projected entangled pair states* can be identified with matrix product unitaries. In the resulting tensor network for evaluating equal-time correlation functions, the bulk ternary unitary gates cancel out. We delineate and implement a numerical algorithm for computing such correlations by contracting the remaining tensors.

DOI: 10.1103/PhysRevLett.130.090601

Introduction.—Dual unitary gates are two-particle gates, some of them chaotic [1], that are unitary both in time and space direction. They form the building blocks of a class of quantum lattice models in 1 + 1 dimensions [2] for which an exact evaluation of different physical quantities such as correlation functions is feasible [2–6]. Since their introduction in [2], dual unitaries have been used to explore different aspects of chaotic many-body systems [6–20] and were realized experimentally [21]. Furthermore, the underlying concept has been extended to tensors with six [22,23] or more legs [24] and quantum channels [25]. Here we generalize the framework to two spatial dimensions, which are known for phenomena not existent in one dimension, like anyons [26,27]. Specifically, we construct and analyze four-particle gates on a square lattice, which are unitary in time and along both spatial dimensions, denoted “ternary unitary” gates. We will show that corresponding quantum lattice models exhibit light ray correlation functions, pictorially along the edges of a pyramid. We also generalize corresponding “solvable” quantum states [3] to two spatial dimensions, assuming cylindrical boundary conditions. In analogy to matrix product states (MPS) in Ref. [3], we employ projected entangled pair states (PEPS) [28,29] as ansatz for the generalization. We will show that these solvable PEPS can be identified with concatenations of matrix product unitaries (MPU) [30,31], a special class of matrix product operators (MPO) [32,33].

Ternary unitary gates.—We examine a subset of four-particle gates $U \in \text{End}(\mathcal{H}^{\otimes 4})$, where \mathcal{H} is the d -dimensional local Hilbert space, usually chosen as $\mathcal{H} = \mathbb{C}^d$, with $d = 2$ for qubits (or spin- $\frac{1}{2}$ particles). The particles are geometrically arranged as a 2×2 plaquette.

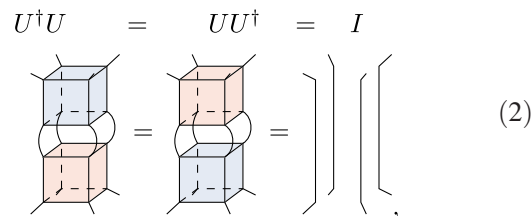
In common tensor network language, U is an 8-tensor, drawn as a cube:



$$U = \text{cube}(1,2,3,4,5,6,7,8), \quad U^\dagger = \text{cube}(1,2,3,4,5,6,7,8). \quad (1)$$

The legs labeled 5, 6, 7, 8 are the input dimensions, and 1, 2, 3, 4 are the output dimensions (conforming with the convention that the leading index of a matrix corresponds to its output). In this picture, the adjoint U^\dagger is a complex-conjugated copy of U mirrored at the spatial $x_1 - x_2$ plane.

We can now define new matrix products \circ_1 and \circ_2 , interpreted as multiplication along the x_1 - and x_2 direction rather than along the t direction. This means contracting different legs compared to the usual matrix product. We define a *ternary unitary* operator U as an operator that is unitary with respect to the usual matrix product and the two products \circ_1 and \circ_2 . Visually, we represent the usual unitary property as



$$U^\dagger U = I, \quad U U^\dagger = I \quad (2)$$

and the unitary condition in the x_1 direction as [34]

$$U^{\dagger 1} \circ_1 U = I \quad U \circ_1 U^{\dagger 1} = I \quad (3)$$

An analogous depiction can be found for the x_2 direction. This definition as cubes is based on the closing thoughts in [2]. A prototypical ternary unitary gate is the generalization of the SWAP gate, denoted “t-SWAP,” swapping the states on opposite sites of a plaquette:

$$U_{\text{t-SWAP}} = \text{[Diagram of a cube with red lines connecting opposite corners]} \quad (4)$$

Constructing ternary unitary gates.—We leave a characterization and encompassing parametrization of ternary unitaries for future work. Here we note that one can construct classes of ternary unitaries from dual unitaries, by combining (possibly different) dual unitary gates, visualized in dark red in the following diagram:

$$U = \text{[Diagram of a cube with red faces]} \quad , \quad U = \text{[Diagram of a cube with red faces]} \quad (5)$$

For example, if we choose all dual unitaries as SWAP gates, both constructions yield the t-SWAP gate. It is straightforward to verify that (5) are indeed ternary unitary. While it is a challenge to find ternary unitary gates directly, dual unitary gates were explicitly parametrized in the qubit case [2] and nongeneral constructions are known for higher dimensions [35]. Notably, the first construction consists of nearest-neighbor gates. Such gates are commonly used in quantum computing to construct other gates [36,37]. An important property of our constructions is that the opposite corners of the cube are connected via interactions.

Physical setting.—We consider a quantum system on a two-dimensional square lattice, where each site is associated with a local Hilbert space $\mathcal{H} = \mathbb{C}^d$. To simplify the discussion, we assume an $L \times L$ lattice with periodic boundary conditions, where L is even. Each site is indexed by coordinates $(i, j) \in (\mathbb{Z}/L)^2$. For conciseness, we denote a 2×2 plaquette anchored at a site $x = (x_1, x_2)$ as $p(x) = \{(x_1, x_2), (x_1 + 1, x_2), (x_1, x_2 + 1), (x_1 + 1, x_2 + 1)\}$. Now define the two operators

$$\mathbb{U}_{\text{ee}} = \bigotimes_{(i,j) \in \{0, \dots, \frac{L}{2}-1\}^2} U_{p(2i, 2j)}, \quad (6)$$

$$\mathbb{U}_{\text{oo}} = \bigotimes_{(i,j) \in \{0, \dots, \frac{L}{2}-1\}^2} U_{p(2i+1, 2j+1)}, \quad (7)$$

where U_S is the ternary unitary U acting on sites S . A motivation for the choice of plaquettes is given in the Appendix, and it can be argued that this pattern is the 2D equivalent of the time evolution used in one dimension [34]. We remark that the following derivations are straightforwardly generalizable for the case of differing ternary gates at each plaquette and time step. In particular, the “light ray” correlation structure (see below) persists. A discrete time step, motivated by trotterized time evolution, is then $\mathbb{U} = \mathbb{U}_{\text{oo}} \mathbb{U}_{\text{ee}}$. The time dependence (in the Heisenberg picture) of a local operator a_x acting on lattice site x is defined as

$$a_x(t) = \mathbb{U}^{-t} a_x \mathbb{U}^t, \quad (8)$$

where t is an integer.

Dynamic correlations.—Based on these definitions, we introduce dynamic correlation functions:

$$D^{\alpha\beta}(x, y, t) = \frac{1}{d^{L^2}} \text{Tr}[a_x^\alpha \mathbb{U}^{-t} a_y^\beta \mathbb{U}^t], \quad (9)$$

with $t \in \mathbb{Z}$ and $\{a_x^\alpha\}_{\alpha=0}^{d^2-1}$ a basis of local operators on \mathcal{H} . We can use the same trick as in the one-dimensional case [2]: Choose $a_x^0 = \mathbb{1}$ and all operators to be Hilbert-Schmidt orthonormal, i.e., $\text{Tr}[a_x^\alpha a_x^\beta] = d\delta_{\alpha\beta}$. Thus all nonidentity operators have trace 0. As immediate consequence $D^{0,0}(x, y, t) = 1$ for all x, y , and t . We find [34] the only remaining cases of nonzero correlations require that a_x^α and a_y^β are connected along a cross-diagonal light ray implying $|x_1 - y_1| = |x_2 - y_2| = 2t$. The tensor diagram then simplifies to the following form (illustrated for $t = 2$):

$$D^{\alpha\beta}(x, y, t) = \frac{1}{d^{6t+1}} \text{[Diagram of a zig-zag chain of cubes for } t=2 \text{]} \quad (10)$$

The open hooked legs are contracted too, but not fully drawn for visual clarity. We can condense (10) further by defining the operator

$$M_z(a) = \frac{1}{d^3} \text{Tr}_{p \setminus \bar{z}} [U^\dagger a_z U], \quad (11)$$

where $p = p(0)$, $z \in p$ indexes one of the sites, and $\bar{z} = (1, 1) - z$. We remark that the maps M_z are d^2 -unistochastic quantum channels [38] and contracting (by an analogous argumentation as in [2]). Finally, we may express the correlation function (in the case of x and y connected by a light ray) as

$$D^{\alpha\beta}(x, y, t) = \frac{1}{d^3} \text{Tr} [M_{y \bmod 2}^{2t}(a^\beta) a^\alpha], \quad (12)$$

where $(y \bmod 2)$ is understood entrywise. Otherwise, $D^{\alpha\beta}(x, y, t) = \delta_{a,b,0}$. Equation (12) is similar to the one-dimensional case [2] and can be computed efficiently with respect to t [34]. Further information on the use of these maps is provided in the Appendix.

Solvable PEPS.—We generalize the concept of solvable states introduced in [3] to two dimensions. The goal is to characterize solvable projected entangled pair states (sPEPS) as initial states, such that a semi-analytic calculation of (equal-time) correlation functions is feasible. Therefore, we consider a scenario that renders the theoretical results in [3] applicable: an $L_1 \times L_2$ square lattice (both L_1 and L_2 even) with cylindrical geometry, i.e., arbitrary boundary conditions in the x_1 direction and periodic boundary conditions in the x_2 direction, and taking the thermodynamic limit $L_1, L_2 \rightarrow \infty$. For the following, a local PEPS tensor Λ represents two neighboring sites in the x_1 direction, endowing it with two physical legs:

$$\Lambda_{\mu_1 \eta_1 \mu_2 \eta_2}^{i,j} = \mu_1 \text{---} \begin{array}{c} i \quad j \\ | \quad | \\ \text{---} \quad \text{---} \\ \eta_1 \quad \eta_2 \end{array} \text{---} \mu_2, \quad (13)$$

here μ (η) denote the virtual bonds parallel to the x_1 (x_2) direction and have bond dimension χ_1 (χ_2). A uniform PEPS corresponding to Λ is shift invariant by two sites in the x_1 direction and one site in the x_2 direction; in short, shift-invariant. We denote the PEPS by $|\Psi_{L_1 L_2}[\Lambda]\rangle$.

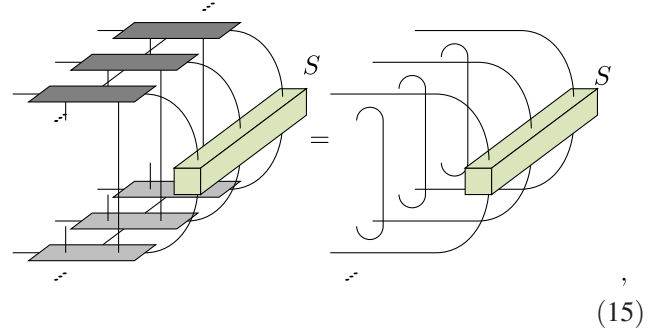
By combining one physical leg with one μ leg each, we can reinterpret Λ as a MPO:

$$\Lambda_{\eta_1 \eta_2}^{(i, \mu_1), (j, \mu_2)} = (i, \mu_1) \text{---} \begin{array}{c} \eta_2 \\ \text{---} \quad \text{---} \\ \eta_1 \end{array} \text{---} (j, \mu_2), \quad (14)$$

where the η legs are the virtual bonds and the other legs correspond to ‘‘physical’’ dimensions. Further, we define

Λ^{L_2} as the contraction of L_2 -many Λ along their ν legs with periodic boundary and call it blocking of local tensors [30]. Now we define two conditions for sPEPS that can be justified by the conditions for solvable MPS [3,34]. A shift-invariant normalized PEPS $|\Psi_{L_1, L_2}[\tilde{\Lambda}]\rangle$ is called solvable if

- (1) The transfer operator of $\tilde{\Lambda}^{L_2}$, defined as the contraction of all physical legs of $\tilde{\Lambda}^{L_2}$ with $(\tilde{\Lambda}^{L_2})^*$, has a unique largest eigenvalue $\lambda = 1$ with an algebraic multiplicity of 1.
- (2) There exists a nonzero tensor $S \in \mathbb{C}^{d^{L_2}} \times \mathbb{C}^{d^{L_2}}$ such that



$$\text{Diagrammatic equation (15)} \quad (15)$$

where the darker local tensors are $\tilde{\Lambda}^*$.

We need two additional definitions to state the following theorem. A matrix product unitary is a MPO such that Λ^{L_2} is unitary for all $L_2 \in \mathbb{N}_1$ [30]. Note that MPUs can be characterized in different ways [30,31]. Secondly, we call two sets of states $\{|\Psi_{L_1 L_2}\rangle\}_{L_1, L_2}$, $\{|\Phi_{L_1 L_2}\rangle\}_{L_1, L_2}$ defined on increasing lattice sizes $L_1 \times L_2$ equivalent (in the thermodynamic limit) if

$$\lim_{L_2 \rightarrow \infty} \lim_{L_1 \rightarrow \infty} \langle \Psi_{L_1 L_2} | \Omega_R | \Psi_{L_1 L_2} \rangle = \lim_{L_2 \rightarrow \infty} \lim_{L_1 \rightarrow \infty} \langle \Phi_{L_1 L_2} | \Omega_R | \Phi_{L_1 L_2} \rangle \quad (16)$$

for all operators Ω_R , where $R \subset \mathbb{Z}^2$ is bounded. Now we can state the main result of this section:

Theorem 1.—Classification of solvable PEPS states. On a square lattice $L_1 \times L_2$ with cylindrical boundary conditions a solvable PEPS $|\Psi_{L_1 L_2}[\tilde{\Lambda}]\rangle$ as defined above is equivalent in the thermodynamic limit to some shift-invariant PEPS $|\Psi_{L_1 L_2}[\Lambda]\rangle$ such that the associated MPO (14) is an MPU up to a scalar factor.

A detailed proof can be found in the Supplemental Material [34]. Essentially, the theorem is a consequence of Theorem 1 in [3] after reducing the two-dimensional lattice geometry to one dimension by grouping all tensors in the x_2 direction at given x_1 and t . In particular, the local Hilbert space dimension is then d^{L_2} .

As a consequence of this theorem, we can restrict the following discussion to PEPS whose local tensors generate a MPU. We study their behavior under the time evolution \mathbb{U} and choose the position of our local tensors Λ such that the first four-particle ternary unitary gates act on plaquettes where each is part of a different Λ , cf. Fig. 1. The

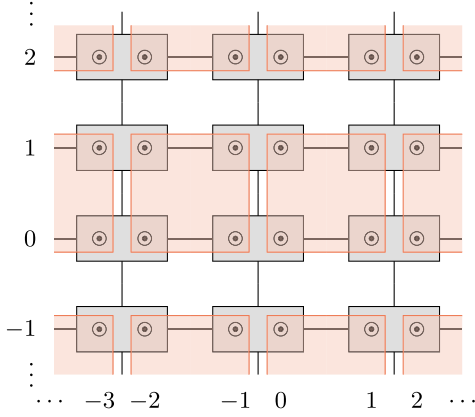


FIG. 1. A top-down view of the PEPS (gray Λ tensors) and the first layer \mathbb{U}_{ee} of ternary unitary gates.

expectation value dynamics of a local operator Ω_R in the thermodynamic limit is

$$E(\Omega_R, t) = \lim_{L_2 \rightarrow \infty} \lim_{L_1 \rightarrow \infty} \langle \Psi_{L_1 L_2} | \mathbb{U}^{-t} \Omega_R \mathbb{U}^t | \Psi_{L_1 L_2} \rangle, \quad (17)$$

where the explicit dependence on Λ was left out. A graphical proof shows that for $\Omega_R = \Omega_{\{x\}}$ a single-site operator $E(\Omega_{\{x\}}, t) = \text{Tr}[\Omega_R]$ for all t . To investigate further we choose $\Omega_R = \Omega_{\{x,y\}}$ to be a two-site operator composed of two single-site operators a_x^α, a_y^β in the same set $\{a^\alpha\}_{\alpha=0}^{d^2-1}$ as before. An immediate consequence of the state normalization is $E(a_x^0, a_y^0, t) = 1$. So assume $\alpha, \beta \neq 0$. Define $r = x - y$ and

$$\Delta = \Delta(x, y) = \min_{\substack{\tilde{x} \in p_x \\ \tilde{y} \in p_y}} |\tilde{x}_2 - \tilde{y}_2|, \quad (18)$$

where $p_z := p(2\lceil(z_1/2)\rceil - 1, 2\lceil(z_2/2)\rceil - 1)$ is a plaquette of four sites. For $r_1, r_2 \geq 0$ we find that Eq. (17), in accordance with [3], is nonzero only if r_1 is sufficiently large and r_2 small enough. Since the proof and the exact solution are very technical and not insightful on their own, they are left to [34]. Note that both in the derivation of the exact solution and for the numerics we assumed the local tensor to be simple [30,34]. The nonzero form can be summarized as the two-single site operators sandwiched in between a big operator and its adjoint. The big operator is a finite number of MPU rows along the x_2 direction and ternary unitaries applied on each end in the x_1 direction on sites forming the face of the light cone of the corresponding operator on top of the cone. Every operator is connected to its adjoint by the identity or a single-site operator. Overall a tube of nontrivial operators is formed. The final result for $\Delta = 0, r_1 = 7$, and $t = 1$ in the form of a tensor network diagram is given in Fig. 2.

Numerical algorithm and simulations.—The computation of the dynamical time-correlation (12) is straightforward, and the specifics of the algorithmic tensor network

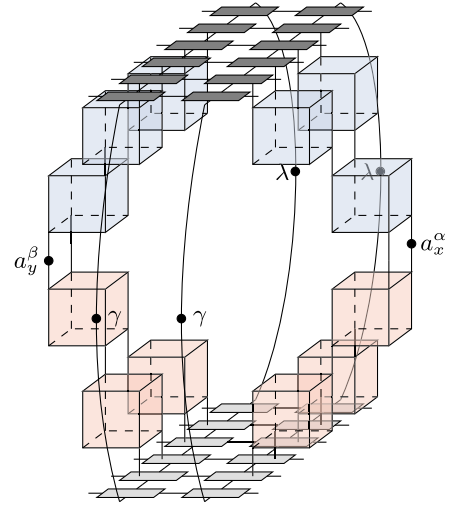


FIG. 2. The tensor network that remains after simplification for the example $\Delta = 0, r_1 = 7$, and $t = 1$. The legs of the unitaries as well as the physical and α legs of the Λ tensors are contracted with the corresponding leg of their adjoint. The tilted triangles in this case each consist of three ternary unitary operators.

contraction visualized in Fig. 2 are left to the Appendix. Fig. 3 visualizes the resulting equal-time correlation functions for $t = 1$. The correlation was taken as the average over two neighboring x_2 positions to avoid even-odd effects. The distance $\Delta x_1 = x_1 - y_1$ has to be odd for the correlation function to be nonzero. Note that we used ternary unitaries in our numerical computations, though the derivation to find a finite tensor network diagram of (17) only requires the four-particle gates to be dual unitary with respect to the x_1 direction. However, the use of ternary unitaries causes a further pattern for which $E(a_x^\alpha, a_y^\beta, t) = 0$ [34]. In general, the computed values fit the theoretical

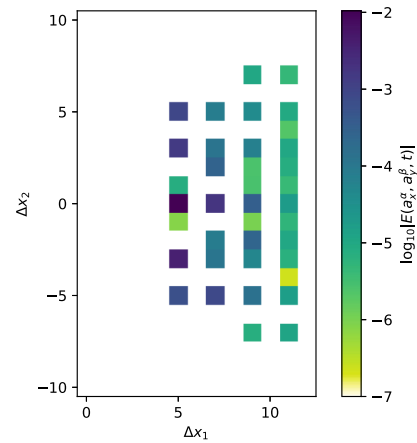


FIG. 3. Equal-time correlation functions for $t = 1$ and a random simple MPU tensor Λ defining the sPEPS, a uniform ternary unitary gate of the form (5), and random traceless local operators a_x^α and a_y^β .

considerations, where the correlation reduces asymptotically for larger distances and is always zero if Δx_2 is above a certain threshold depending on Δx_1 .

Discussion and outlook.—A new class of four-particle gates called ternary unitary gates was introduced in this work. While we gave two possible ways to construct them from dual unitaries, it would be desirable to find the most general parametrization. We expect that further connections with quantum information theory will become apparent in the future, analogous to dual unitaries [18,19]. Additionally, since many current quantum computing architectures use two-dimensional geometries [39–41], ternary unitaries may explore their limitations. Other aspects to be explored could take inspiration from the works of recent years considering dual unitaries. Among such topics of interest are entanglement dynamics [3,7,11,13] and the approximation of dual unitaries [8,9,20]. Most likely, two-spatial dimensions give rise to interesting new phenomena and challenges, in particular regarding topological aspects.

Note that the results obtained for the expectation value dynamics are a generalization of the results found in [42]. They confined themselves to solvable states with $\chi_2 = 1$, obtaining nonzero E only in the case of $r_2 = 0$. Since the MPUs are well-studied objects, their known properties can be used to analyze the solvable PEPS further. However, one might not consider MPUs the best ansatz for a solvable state, since the treatment of the two spatial dimensions is asymmetric. Notably, the limits in Eq. (17) do not commute, and in our derivation it is sufficient to assume the operators U to be dual unitary in the x_1 direction.

We thank Frank Pollmann and Toby Cubitt for inspiring discussions. The research is part of the Munich Quantum Valley, which is supported by the Bavarian State Government with funds from the Hightech Agenda Bayern Plus.

Appendix A: Motivation of the physical setting.—For the left construction in Eq. (5) we can motivate the setting as a trotterized time evolution governed by a Hamiltonian with nearest neighbor interactions:

$$\mathbb{U} = \mathbb{U}_{\text{oo,vert}} \mathbb{U}_{\text{oo,horz}} \mathbb{U}_{\text{ee,vert}} \mathbb{U}_{\text{ee,horz}}. \quad (\text{A1})$$

Here $\mathbb{U}_{\text{ee,horz}}$ is the interaction between even-indexed sites with their right neighbors, and $\mathbb{U}_{\text{ee,vert}}$ with their upper neighbors. Analogously, $\mathbb{U}_{\text{oo,vert}}$ and $\mathbb{U}_{\text{oo,horz}}$ start from odd-indexed sites. The operators consist of nonoverlapping two-particle gates, see Fig. 4. If we choose these gates as dual unitaries, we can combine them to form ternary unitary gates as in Eq. (5):

$$\mathbb{U}_{\text{ee}} = \mathbb{U}_{\text{ee,vert}} \mathbb{U}_{\text{ee,horz}}, \quad \mathbb{U}_{\text{oo}} = \mathbb{U}_{\text{oo,vert}} \mathbb{U}_{\text{oo,horz}}. \quad (\text{A2})$$

They can then be used in the evolution \mathbb{U} . The choice of which gates to combine is basically a repartitioning of

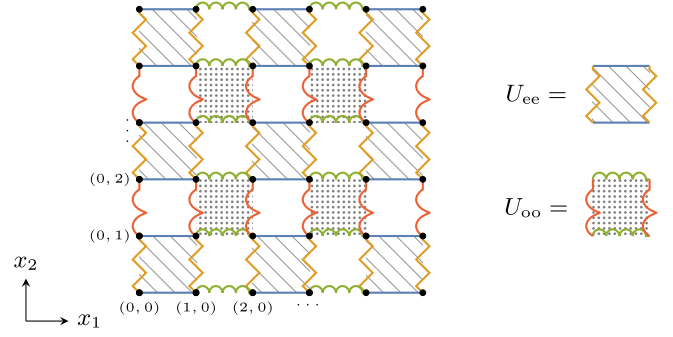


FIG. 4. Pattern sequence of dual unitary gates which can be subsumed as two “time steps” of ternary unitary gates of the form (5).

supercells for quantum cellular automata (QCA) [43] and the same partitionings as used in [44]. \mathbb{U}_{ee} and \mathbb{U}_{oo} are the corresponding QCA to each partitioning and motivate the first construction in Eq. (5). Notably, QCAs have been used to analyze Floquet systems [43] and gave rise to the concept of dual-unitary operators in the process [2,45,46].

Appendix B: Unistochastic M Maps.—This appendix has further information on the contracting maps introduced in Eq. (11). First, we provide a visual example to aid the intuition:

$$M_{(1,1)}(a) = \frac{1}{d^3} \quad (\text{B1})$$

Furthermore, note that we can simplify Eq. (12) further, by writing it in the form

$$D^{\alpha\beta}(x, y, t) = \sum_{\chi=0}^{d^2-1} c_{y,x}^{\alpha\beta}(t) \lambda_{y,x}^{2t}, \quad (\text{B2})$$

where $\{\lambda_{y,x}\}_{\chi=0}^{d^2-1}$ are the eigenvalues of $M_{y \bmod 2}$ and $c_{y,x}^{\alpha\beta}(t)$ are polynomials in t . The eigenvalues lie on the unit disk and have coinciding algebraic and geometric multiplicity if they are on the unit circle [2]. This result is analogous to those in [2] and shows that the eigenvalues suffice to classify ternary unitaries by their ergodicity. Refer to [34] for a detailed analysis of the M maps for the specific constructions (5).

Appendix C: Numerical algorithms.—We computed the nonzero dynamical correlation function (9) by interpreting the network (10) as the expectation value of a M^n with

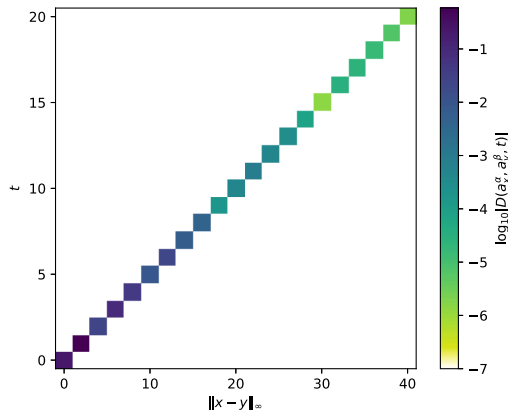


FIG. 5. The dynamical correlation function for a uniform ternary unitary gate of the form (5), and random traceless local operators a_x^α and a_y^β .

respect to the vectors a_x^α and a_y^β . The results can be seen in Fig. 5. While the correlation does not fall monotonously with time (or distance), it decreases asymptotically. This fits with the results one would expect according to (B2) and the results obtained in [12] for dual unitary operators.

The task of computing the final tensor network representing the expectation value dynamics is split into two steps: (1) The conjugations by ternary unitaries of the local operators a_x^α and a_y^β are represented as two MPOs, respectively. Specifically, we start from a MPO representation of the identity with a length equal to the extent in the x_2 direction, substitute the local operators a_x^α and a_y^β , and then apply the maps ternary unitaries in a TEBD-type brick-wall pattern. Just like the M maps the resulting operators are contractive, so one expects only a modest increase of entanglement. The two final MPOs are sandwiched between the PEPS tensors on the left and right boundary. (2) The PEPS tensors are first contracted along the physical legs with their conjugated copy while inserting the MPOs from step 1 on the left and right boundary, and MPU ring transfer states on the top and bottom boundary. This leads to a two-dimensional grid of new tensors connected by virtual bonds in each of the four spatial directions. Finally, this network is then contracted row by row or column by column. We remark that the last substep is affected by the “curse of dimensionality” for increasing distance $|x_1 - y_1|$.

* r.milbradt@tum.de

† lisa.scheller@tum.de

‡ chris.assmus@tum.de

§ christian.mendl@tum.de

[1] B. Bertini, P. Kos, and T. Prosen, Random matrix spectral form factor of dual-unitary quantum circuits, *Commun. Math. Phys.* **387**, 597 (2021).

[2] B. Bertini, P. Kos, and T. Prosen, Exact Correlation Functions for Dual-Unitary Lattice Models in $1+1$ Dimensions, *Phys. Rev. Lett.* **123**, 210601 (2019).

[3] L. Piroli, B. Bertini, J.I. Cirac, and T. Prosen, Exact dynamics in dual-unitary quantum circuits, *Phys. Rev. B* **101**, 094304 (2020).

[4] B. Gutkin, P. Braun, M. Akila, D. Waltner, and T. Guhr, Local correlations in dual-unitary kicked chains, *arXiv:2001.01298*.

[5] Y. Kasim and T. Prosen, Dual unitary circuits in random geometries, *arXiv:2206.09665*.

[6] P. W. Claeys and A. Lamacraft, Maximum velocity quantum circuits, *Phys. Rev. Res.* **2**, 033032 (2020).

[7] B. Bertini, P. Kos, and T. Prosen, Operator entanglement in local quantum circuits I: Chaotic dual-unitary circuits, *SciPost Phys.* **8**, 067 (2020).

[8] S. A. Rather, S. Aravinda, and A. Lakshminarayan, Creating Ensembles of Dual Unitary and Maximally Entangling Quantum Evolutions, *Phys. Rev. Lett.* **125**, 070501 (2020).

[9] P. Kos, B. Bertini, and T. Prosen, Correlations in Perturbed Dual-Unitary Circuits: Efficient Path-Integral Formula, *Phys. Rev. X* **11**, 011022 (2021).

[10] P. Kos, B. Bertini, and T. Prosen, Chaos and Ergodicity in Extended Quantum Systems with Noisy Driving, *Phys. Rev. Lett.* **126**, 190601 (2021).

[11] I. Reid and B. Bertini, Entanglement barriers in dual-unitary circuits, *Phys. Rev. B* **104**, 014301 (2021).

[12] P. W. Claeys and A. Lamacraft, Ergodic and Nonergodic Dual-Unitary Quantum Circuits with Arbitrary Local Hilbert Space Dimension, *Phys. Rev. Lett.* **126**, 100603 (2021).

[13] A. Foligno and B. Bertini, Growth of entanglement of generic states under dual-unitary dynamics, *arXiv:2208.00030*.

[14] D. T. Stephen, W. W. Ho, T.-C. Wei, R. Raussendorf, and R. Verresen, Universal measurement-based quantum computation in a one-dimensional architecture enabled by dual-unitary circuits, *arXiv:2209.06191*.

[15] M. A. Rampp, R. Moessner, and P. W. Claeys, From dual unitarity to generic quantum operator spreading, *arXiv:2210.13490*.

[16] S. Brahmachari, R. N. Rajmohan, S. A. Rather, and A. Lakshminarayan, Dual unitaries as maximizers of the distance to local product gates, *arXiv:2210.13307*.

[17] A. Zabalo, M. J. Gullans, J. H. Wilson, R. Vasseur, A. W. W. Ludwig, S. Gopalakrishnan, D. A. Huse, and J. H. Pixley, Operator Scaling Dimensions and Multifractality at Measurement-Induced Transitions, *Phys. Rev. Lett.* **128**, 050602 (2022).

[18] S. A. Rather, A. Burchardt, W. Bruzda, G. Rajchel-Mieldzióć, A. Lakshminarayan, and K. Życzkowski, Thirty-Six Entangled Officers of Euler: Quantum Solution to a Classically Impossible Problem, *Phys. Rev. Lett.* **128**, 080507 (2022).

[19] K. Życzkowski, W. Bruzda, G. Rajchel-Mieldzióć, A. Burchardt, S. A. Rather, and A. Lakshminarayan, $9 \times 4 = 6 \times 6$: Understanding the quantum solution to the Euler’s problem of 36 officers, *arXiv:2204.06800*.

[20] T. Zhou and A. W. Harrow, Maximal entanglement velocity implies dual unitarity, *Phys. Rev. B* **106**, L201104 (2022).

- [21] E. Chertkov, J. Bohnet, D. Francois, J. Gaebler, D. Gresh, A. Hankin, K. Lee, D. Hayes, B. Neyenhuis, R. Stuz, A. C. Potter, and M. Foss-Feig, Holographic dynamics simulations with a trapped-ion quantum computer, *Nat. Phys.* **18**, 1074 (2022).
- [22] T. Prosen, Many-body quantum chaos and dual-unitarity round-a-face, *Chaos* **31**, 093101 (2021).
- [23] C. Jonay, V. Khemani, and M. Ippoliti, Triunitary quantum circuits, *Phys. Rev. Res.* **3**, 043046 (2021).
- [24] M. Mestyán, B. Pozsgay, and I. M. Wanless, Multi-directional unitarity and maximal entanglement in spatially symmetric quantum states, [arXiv:2210.13017](https://arxiv.org/abs/2210.13017).
- [25] P. Kos and G. Styliaris, Circuits of space-time quantum channels, [arXiv:2206.12155](https://arxiv.org/abs/2206.12155).
- [26] A. Y. Kitaev, Fault-tolerant quantum computation by anyons, *Ann. Phys. (Amsterdam)* **303**, 2 (2003).
- [27] A. Y. Kitaev, Anyons in an exactly solved model and beyond, *Ann. Phys. (Amsterdam)* **321**, 2 (2006).
- [28] F. Verstraete and J. I. Cirac, Renormalization algorithms for quantum-many body systems in two and higher dimensions, [arXiv:cond-mat/0407066](https://arxiv.org/abs/cond-mat/0407066).
- [29] M. B. Hastings, Solving gapped Hamiltonians locally, *Phys. Rev. B* **73**, 085115 (2006).
- [30] J. I. Cirac, D. Perez-Garcia, N. Schuch, and F. Verstraete, Matrix product unitaries: Structure, symmetries, and topological invariants, *J. Stat. Mech.* (2017) 083105.
- [31] M. B. Şahinoğlu, S. K. Shukla, F. Bi, and X. Chen, Matrix product representation of locality preserving unitaries, *Phys. Rev. B* **98**, 245122 (2018).
- [32] F. Verstraete, V. Murg, and J. I. Cirac, Matrix product states, projected entangled pair states, and variational renormalization group methods for quantum spin systems, *Adv. Phys.* **57**, 143 (2008).
- [33] G. K.-L. Chan, A. Keselman, N. Nakatani, Z. Li, and S. R. White, Matrix product operators, matrix product states, and *ab initio* density matrix renormalization group algorithms, [arXiv:1605.02611](https://arxiv.org/abs/1605.02611).
- [34] See Supplemental Material at <http://link.aps.org/supplemental/10.1103/PhysRevLett.130.090601> it contains more technical aspects of the definition of ternary unitary operators. Furthermore, details on the calculations of the correlation functions and expectation value dynamics, and the numerical computations performed in this work can be found.
- [35] M. Borsi and B. Pozsgay, Remarks on the construction and the ergodicity properties of dual unitary quantum circuits, *Phys. Rev. B* **106**, 014302 (2022).
- [36] A. Bhattacharjee, C. Bandyopadhyay, R. Wille, R. Drechsler, and H. Rahaman, A novel approach for nearest neighbor realization of 2D quantum circuits, *IEEE Computer Society Annual Symposium on VLSI* (IEEE, Hong Kong, 2018), p. 305, [10.1109/ISVLSI.2018.00063](https://doi.org/10.1109/ISVLSI.2018.00063).
- [37] A. Bhattacharjee and H. Rahaman, An efficient 2D mapping of quantum circuits to nearest neighbor designs, *IEEE International Symposium on Smart Electronic Systems* (2021), p. 53, [10.1109/iSES52644.2021.00024](https://doi.org/10.1109/iSES52644.2021.00024).
- [38] M. Musz, M. Kuś, and K. Życzkowski, Unitary quantum gates, perfect entanglers, and unistochastic maps, *Phys. Rev. A* **87**, 022111 (2013).
- [39] F. Arute, K. Arya, R. Babbush *et al.*, Quantum supremacy using a programmable superconducting processor, *Nature (London)* **574**, 505 (2019).
- [40] A. J. Park, J. Trautmann, N. Šantić, V. Klüsener, A. Heinz, I. Bloch, and S. Blatt, Cavity-enhanced optical lattices for scaling neutral atom quantum technologies to higher qubit numbers, *PRX Quantum* **3**, 030314 (2022).
- [41] T. M. Graham *et al.*, Multi-qubit entanglement and algorithms on a neutral-atom quantum computer, *Nature (London)* **604**, 457 (2022).
- [42] R. Suzuki, K. Mitarai, and K. Fujii, Computational power of one- and two-dimensional dual-unitary quantum circuits, *Quantum* **6**, 631 (2022).
- [43] T. Farrelly, A review of quantum cellular automata, *Quantum* **4**, 368 (2020).
- [44] R. Raussendorf, Quantum cellular automaton for universal quantum computation, *Phys. Rev. A* **72**, 022301 (2005).
- [45] B. Bertini, P. Kos, and T. Prosen, Exact Spectral Form Factor in a Minimal Model of Many-Body Quantum Chaos, *Phys. Rev. Lett.* **121**, 264101 (2018).
- [46] B. Bertini, P. Kos, and T. Prosen, Entanglement Spreading in a Minimal Model of Maximal Many-Body Quantum Chaos, *Phys. Rev. X* **9**, 021033 (2019).